Austrian Journal of Earth Sciences | Volume 104/1 | 36 - 48 | Vienna | 2011

Mineralogy, mineral chemistry and petrology of the Ag-bearing Cu-Fe-Pb-Zn sulfide mineralizations of the Pfunderer Berg (South Tyrol, Italy)

Matthias KRISMER*), Franz VAVTAR, Peter TROPPER, Bernhard SARTORY & Reinhard KAINDL

KEYWORDS

Cu-Fe-Pb-Zn deposit
Pfunderer Berg
South Tyrol
tetrahedrite
polybasite
freibergite
acanthite
gustavite
electrum
cosalite

Institute of Mineralogy and Petrography, Faculty of Geo- and Atmospheric Sciences, University of Innsbruck, Innrain 52, A-6020 Innsbruck, Austria;

*) Corresponding author, matthias.krismer@uibk.ac.at

Abstract

The Cu-Fe-Pb-Zn-(Ag) deposit of the Pfunderer Berg is located near the Eisack Valley, northwest of Klausen in South Tyrol, Italy. The mineralizations are hosted in the rocks of the Southalpine Basement and are related to Permian dioritic intrusions. The observed primary sulfide assemblage consists of galena + chalcopyrite + sphalerite + freibergite-tetrahedrite$_{ss}$ ± polybasite ± acanthite ± electrum. The most common Ag-bearing phases are freibergite-tetrahedrite$_{ss}$, polybasite and acanthite. They occur as few microns-large, pebble-shaped inclusions in galena. The most common inclusions are freibergite and freibergite-tetrahedrite$_{ss}$ followed by polybasite and acanthite. In one sample intimately intergrown gustavite ($AgPbBi_3S_6$) and cosalite ($Pb_2Bi_2S_5$) were found. These two rare minerals have been described for the first time at the Pfunderer Berg. Rarely electrum occurs as inclusion in chalcopyrite. Chalcopyrite shows anisotropic transformation lamellae as well as numerous star-shaped sphalerite inclusions. Sphalerite shows replacement textures by chalcopyrite, contains chalcopyrite inclusions and also shows complex Cu-Fe zoning patterns. Idiomorphic pyrite, dispersed throughout the samples, and a second generation of tetrahedrite (secondary tetrahedrite) represent the secondary sulfide assemblage, which crystallized after the main mineralization stage.

Sphalerite inclusions in chalcopyrite, interpreted as exsolutions from a ZnS-bearing high-T ISS phase during cooling, as well as α-β transformation lamellae in chalcopyrite indicate high temperatures of formations >500°C for the formation of the primary sulfide assemblage. Cd-exchange thermometry between galena and sphalerite yielded temperatures between 500°C and 900°C. Due to the associated uncertainties these values represent only semiquantitative information but confirm the high-T formation of the primary sulfide assemblage associated with Permian magmatic activities and agree with the observed cooling textures. Old mining records frequently mention the high Ag content of the minerals of this deposit and galena was considered as the dominant Ag-bearing mineral. It could be shown in this study that the presence of abundant Ag-rich mineral inclusions in galena is responsible for the high Ag concentrations of bulk galena.

These mineralogical data are the prerequisite concerning possible provenance studies of ores used in the prehistoric Cu production in the Southern Alps in the course of the special research area HiMAT (History of Mining in the Tyrol and Adjacent Areas). The implications are that Cu-slags and metal compositions produced by smelting of the chalcopyrite-sphalerite-galena-rich ores from the Pfunderer Berg should show a characteristic, but different chemical signature from fahlore-based products from the lower Inn valley due the complex phase assemblage in the system Cu-Fe-Pb-Zn and the elevated Ag contents.

Die Cu-Fe-Pb-Zn-(Ag) Lagerstätte Pfunderer Berg liegt in der Nähe des Eisacktals bei Klausen (Südtirol). Die Lagerstätte befindet sich in den Gesteinen des Südalpins und ist genetisch mit den permischen Dioritintrusionen von Klausen verwand. Die primäre Sulfidparagenese setzt sich aus Galenit + Chalcopyrit + Sphalerit + Freibergit-Tetraedrit$_{ss}$ zusammen. Als Nebengemengeteile findet man Polybasit, Akanthit und Elektrum. Die Ag Erze Freibergit-Tetraedrit$_{ss}$, Polybasit und Akanthit treten in Form von winzigen, tropfenförmigen Einschlüssen im Galenit auf. Der größte Teil der Einschlüsse setzt sich aus Freibergit-Tetraedrit$_{ss}$, gefolgt von Polybasit und Akanthit zusammen. In einer Probe wurden Cosalit ($Pb_2Bi_2S_5$) und Gustavit ($AgPbBi_3S_6$) als schmale Anwachsäume von Chalcopyrit festgestellt. Das Auftreten dieser beiden Phasen am Pfunderer Berg wird hier zum ersten Mal beschrieben. Elektrum tritt sehr selten als Einschluss im Chalcopyrit auf, welcher häufig oleanderblattförmige α-β Umwandlungslamellen und zahlreiche, sternförnige Zinkblende Einschlüsse aufweist. Sphalerit wird häufig von Chalcopyrit verdrängt, enthält zahlreiche tropfenförmige Chalcopyrit Einschlüsse und zeigt komplexe Cu-Fe Zonierungen. Idiomorpher Pyrit und eine zweite Ag-arme und As-reiche Tetraedritgeneration stellen aufgrund der Wachstumstexturen die sekundäre Mineralparagenese dar, die später als die primäre Mineralparagenese gewachsen ist. Sternförmige Sphalerit Einschlüsse in Chalcopyrit werden als ZnS Entmischungen aus einer hoch-T ISS Phase während der Abkühlung interpretiert. Die α-β Umwandlungslamellen in Kupferkies werden ebenfalls als Abkühlungstexturen interpretiert. Die beschriebenen Texturen lassen auf Entstehungstemperaturen >500°C schließen. Das Cd-Austauschthermo-

meter zwischen Sphalerit und Galenit ergibt trotz großer Streuung einen Temperaturbereich von 500°C bis 900°C was auch auf die Hoch-T Bildung der Lagerstätte in Zusammenhang mit den Permischen Intrusionen hinweist. In der älteren Literatur wird vor allem der Ag Reichtum der Lagerstätte hervorgehoben, wobei Bleiglanz als Ag Träger vermutet wurde. In dieser Untersuchung konnte nachgewiesen werden, dass Polybasit, Freibergit und Acanthit Einschlüsse in Galenit dafür verantwortlich sind.

Diese mineralogischen Daten bilden die Basis für zukünftige Herkunftsstudien bezüglich prähistorischer Cu Rohstoffe im Südalpinen Raum im Rahmen des Sonderforschungsbereiches HiMAT (History of Mining in the Tyrol and Adjacent Areas). Es kann erwartet werden, dass durch die Verhüttung der Chalcopyrit-Sphalerit-Galenit-reichen Erze vom Pfunderer Berg, aufgrund der komplexen mineralogischen/chemischen Zusammensetzung im System Cu-Fe-Pb-Zn und den hohen Ag Gehalten, charakteristische Metall- und Schlackenzusammensetzungen produziert werden, die sich von Produkten auf Fahlerzbasis aus dem unteren Inntal deutlich unterscheiden.

1. Introduction

Mining archaeological investigations revealed that various Cu deposits in the Southern Alps were mined from the middle Bronze Age on and probably also before (Metten, 2003). Unfortunately, archaeological investigations concerning the extent and the intensity of these prehistoric mining activities in the Southern Alps are far from conclusive yet. The most important Bronze Age mining and smelting activities were described from the autonomous Italian province of Trentino with the smelting centre in Aqua Fredda, approximately 20 km to the northeast of the city of Trento (Metten, 2003). Although several large Cu-deposits are known further north in the autonomous Italian province South Tyrol, no definitive evidence for prehistoric mining activities has been found in South Tyrol yet. The special research program HiMAT (Historical Mining Activities in the Tyrol and Adjacent Areas), installed at the University of Innsbruck (Oeggl et al., 2008), will address the topic of prehistoric and historic Cu-mining activities in the Southern Alps, with a focus on selected South Tyrolean sites associated with Cu ore deposits. Thus the first step in the exploration of possible prehistoric mining and smelting activities in an area is the mineralogical, petrological and geochemical characterization of possible adjacent ore deposits (e.g. Niederschlag et al., 2003). These results can then be used as a basis for subsequent mining archaeological investigations in order to conduct raw material provenance studies as well as interpretations concerning the smelting technologies used (e.g. Niederschlag et al., 2003).

The Pfunderer Berg mining district is a historic and probably also a prehistoric mining area (Krismer et al., 2008). First mentioned in 1140, the last mining activities were aborted in 1943 (Dorfmann, 1974). Old mining records frequently mention the high silver content of the minerals of this deposit and galena was considered as the dominant silver-bearing mineral (Moll, 1798; Dorfmann, 1974), but mineralogical and mineral chemical data are completely lacking so far. This study represents therefore the first electron microprobe investigation of the sulfide mineral assemblage from this deposit.

The aims of this work are therefore fourfold, namely to 1.) provide a detailed overview of the sulfide matrix mineral and inclusion assemblages, 2.) obtain their chemical composition with a special focus on the nature and occurrence of the Ag-bearing sulfides, 3.) deduce T-fS_2 conditions of primary sulfide formation and 4.) discuss the implications of the chemical data for future prehistoric ore provenance studies in the course of the special research area HiMAT (History of Mining in the Tyrol and Adjacent Areas).

2. Geological overview

The Pfunderer Berg is located to the west of Klausen in the autonomous Italian province of South Tyrol (Figure 1). The geomorphology of the area is characterized by the narrow Thinne creek, marking the north-eastern boundary of the mining area. To the south-west the steep slope of the Villanderer Berg extends from the Thinne creek approximately 750 m a.s.l. to the

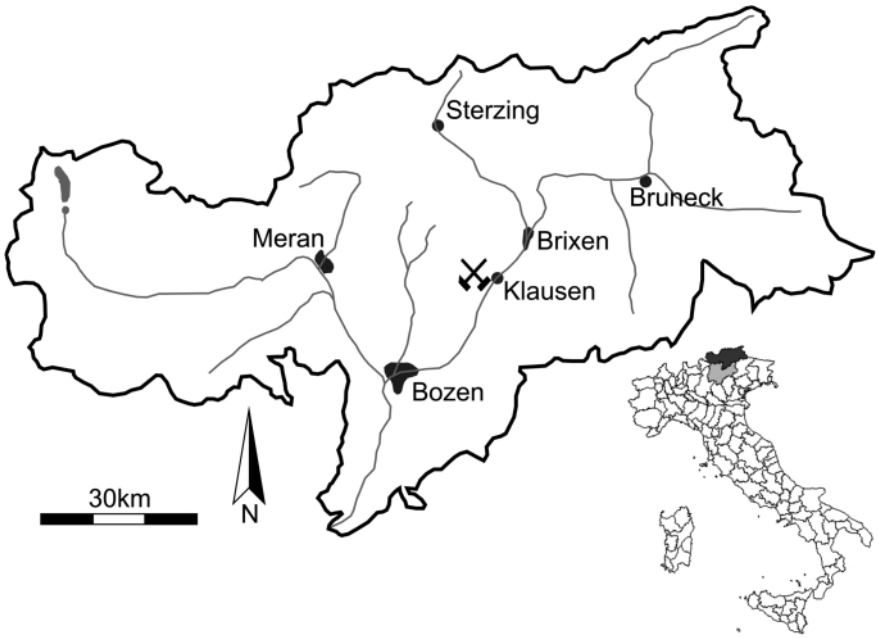

Figure 1: Geographic map of South Tyrol, the mining symbol marks the location of the Pfunderer Berg. The mining district of the Pfunderer Berg is located to the west of Klausen/Chiusa between Bozen/Bolzano and Brixen/Bressanone.

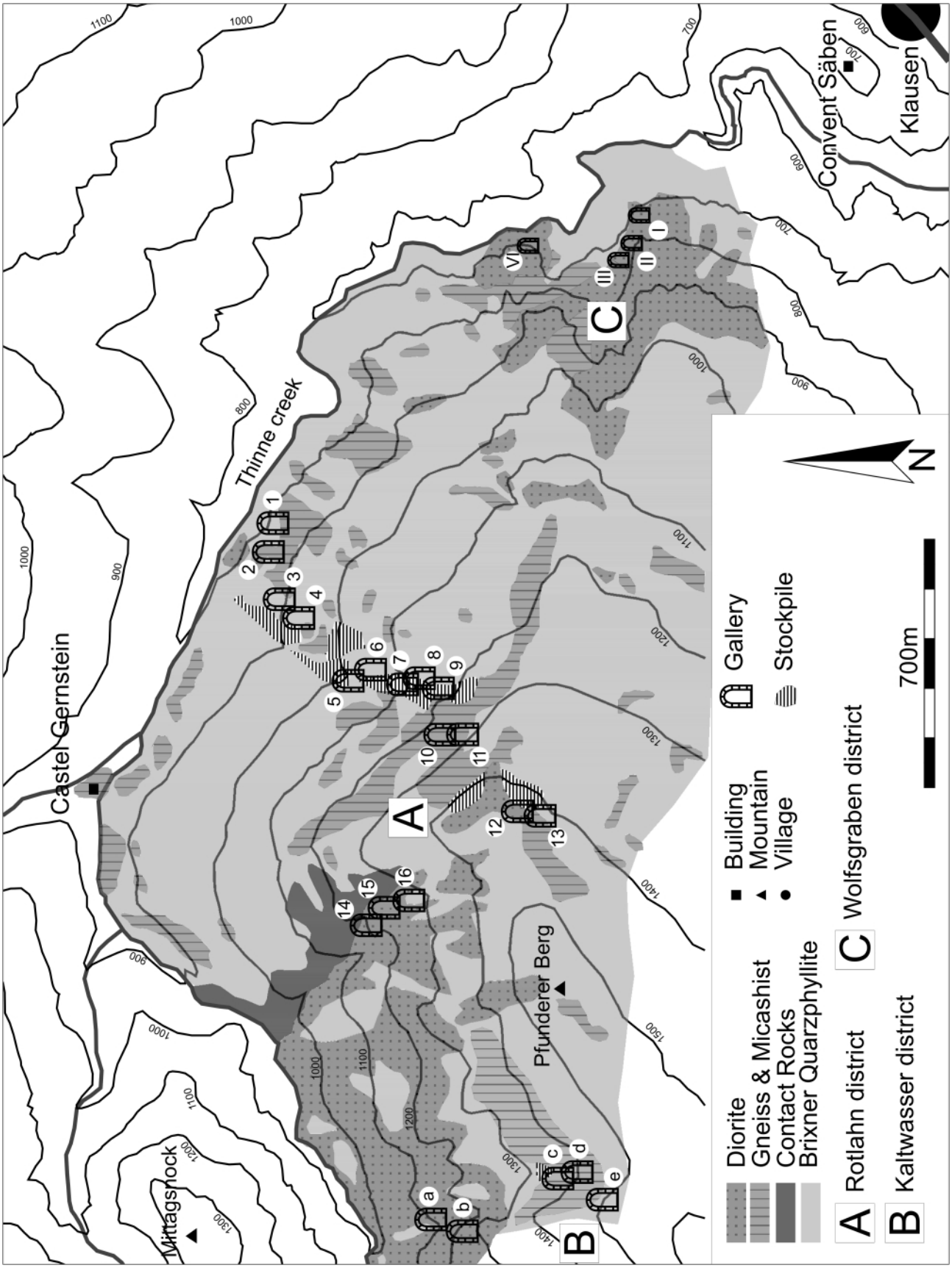

Figure 2: Geological overview of the Pfunderer Berg mining district, modified after Exel (1998). The numbers in the white circles denote the exit mouths of galleries. The galleries are named according to Exel (1998). A = Rotlahn district: 1) Hirschlegg-Stollen, 2) Vittorio Emanuele-Stollen, 3) Franz-Stollen, 4) Theresia-Stollen, 5) Katharina-Stollen, 6) Kassian-Stollen, 7) Barbara-Stollen, 8) Andreas-Stollen, 9) Nikolaus-Stollen, 10) Elisabeth-Stollen, 11) Lorenz-Stollen, 12) Fundgrube, 13) Kreuz-Stollen, 14) Martin Stollen, 15) Mathias-Stollen, 16) Georg Stollen. B = Kaltwasser District: a) Remedi-Stollen, b) Tagebau, c) Unterer Kaltwasser-Stollen, d) Oberer Kaltwasser-Stollen, e) Tagebau. C = Wolfsgraben Distric: I, II, III, IV (no specific names in the literature).

peak of the Pfunderer Berg at 1519 m a.s.l. (Figure 2). The ore deposits are situated in the rocks of the Southalpine crystalline basement. The dominant basement lithology near Klausen is the Brixen Quarzphyllite (Figure 2), which was intruded by Permian small dioritic intrusion bodies or dykes leading to widespread contact metamorphism. These dioritic rocks have been called Klausenites. The ore deposits are located either in the dioritic dikes, in the contact area between the intrusive rocks and the basement rocks, or in the contact metamorphic rocks, the hornfelses (Figure 2). The mining district is located to the south of the SAM (Southern limit of Alpine Metamorphism, Hoinkes et al., 1999), which indicates that the basement and the ore mineralizations were not, or only very weakly, affected by Alpine metamorphism. However, despite the lack of significant Alpine metamorphic overprint, the area south of the SAM experienced Alpine folding and faulting (Sassi and Spiess, 1993) which led at least in part to secondary remobilization of the ore deposits (Dorfmann 1974).

The Cu-Fe-Pb-Zn-(Ag) mineralizations of the Pfunderer Berg formed due to hydrothermal processes related to the diorite intrusions in the area of Klausen (Exel, 1998; Fuchs, 1988). The Pfunderer Berg is part of several Pb-Zn-Cu-Fe-(Ag) mineralizations occurring in the contact area between the Permian granitic- to dioritic Intrusions and the Southalpine basement in the area of Brixen and Meran, South Tyrol (Fuchs, 1988). The main sulfide assemblage described by Dorfmann (1974) and Exel (1998) consists of galena, sphalerite, pyrite, chalcopyrite and fahlore-group minerals. Accessory sulfide minerals are electrum, polybasite and acanthite. Besides these phases a number of additional minerals such as marcasite, arsenopyrite, antimonite (stibnite), jamesonite, boulangerite, gudmundite, pyargirite, native gold (Dorfmann, 1974) as well as native silver (Posepny, 1880) and molybdenite (Klebelsberg, 1935) have been described in the literature. Native gold occurring as inclusions in pyrite and sphalerite was described by Brigo (1971). Oxide ore minerals are hematite, which occurs as inclusions in pyrite and magnetite as well as in sphalerite (Dorfmann, 1974). In the different lithologies (diorite, hornfelses and quartzphyllites) the ore mineral assemblage is different. Whereas quartzphyllites and contact metamorphic rocks predominantly contain chalcopyrite and pyrite, the intrusive rocks contain galena and sphalerite. However, these four phases also occur together in many samples. Gangue phases are mostly quartz but occasionally calcite, barite and fluorite occur (Dorfmann, 1974).

3. Analytical techniques

Due to the lack of appropriate samples from the now abandoned Pfunderer Berg mine, samples were taken from the ore collection of the Institute of Mineralogy and Petrolography of the University of Innsbruck and only samples with known geographical provenance were used. Selected samples were prepared as polished sections. For polarized light microscopical investigations a Leica DM 2500P microscope with reflected light mode as well as transmitted light mode was used. Standard electron microprobe analysis was carried out using the JEOL JXA 8100 SUPERPROBE with five WDS detectors and a Thermo Noran EDS system. The analyses file contained the elements S, Cu, Fe, Zn, Hg, Mn, Mo, Cd, Ni, Pb, Co, Au, Ag, Ge, In, As, Sb, Bi, Se, Sn, Te. Eleven peak overlap corrections were considered in order to minimize interferences between the various elements. For further phase information micro-Raman spectroscopy was applied using a HORIBA JOBIN YVON LabRam-HR 800 Raman micro-spectrometer. Samples were excited at room temperature with the 515 nm emission line of an Ar-ion laser through an OLYMPUS 100X objective.

4. Ore petrography and textural relations

The sulfide mineral assemblage consists of galena + chalcopyrite + sphalerite + pyrite + secondary tetrahedrite + freibergite-tetrahedrite$_{ss}$ ± polybasite ± acanthite ± electrum. All samples are characterized by numerous idiomorphic secondary pyrite grains overgrowing the primary phase assemblage. A second generation of Ag-poorer, As-richer tetrahedrite coexists with pyrite (secondary tetrahedrite). From textural relations both, pyrite and secondary tetrahedrite were formed in a later stage of the ore forming process. One sample also contains the rare phases cosalite and gustavite, two Bi-Pb-(Ag) sulfides with the formulae $Pb_2Bi_2S_5$ and $AgPbBi_3S_6$, respectively. Table 1 shows the phase assemblages of all 15 investigated samples.

Ag-Au-rich phases: Besides electrum, Ag-bearing minerals are only present as tiny lenticular- and pebble-shaped inclusions in large galena grains (Figure 3). The most common Ag-phase is freibergite-tetrahedrite$_{ss}$ followed by polybasite and acanthite. The size of the Ag-rich inclusions varies from only a few microns up to 50 microns. Freibergite-tetrahedrite$_{ss}$ pebbles are greenish-grey (Figure 3), show no pleochroism and are isotropic. Polybasite appears bluish (Figure 3) with distinct pleochroism. The anisotropy of polybasite is well visible. While freibergite-tetrahedrite$_{ss}$ and polybasite are com-

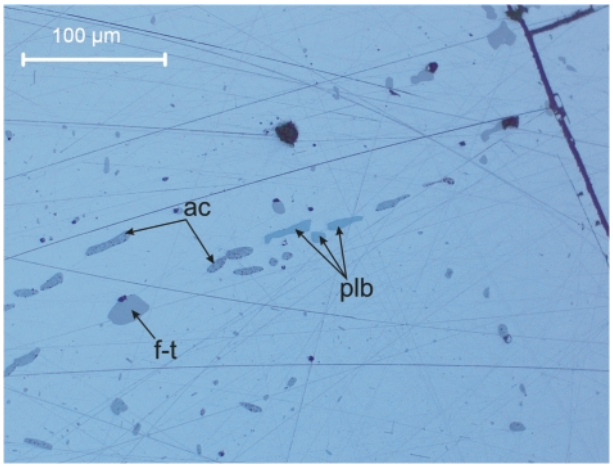

Figure 3: Reflected light microphotograph showing freibergite-tetrahedrite$_{ss}$, polybasite and acanthite inclusions in galena. Abbreviations: ac: acanthite, plb: polybasite, f-t: freibergite-tetrahedrite$_{ss}$.

mon, acanthite is rare and exhibits strongly corroded surfaces (Figure 3). These inclusions were formed during a primary mineralization stage. Electrum was very rarely found. The grains are enclosed in chalcopyrite. The textural appearance suggests that electrum also formed during the primary mineralization stage.

Bi-(Ag) phases: Gustavite and cosalite are Bi-bearing phases which were found in one sample as distinct rims surrounding chalcopyrite (Figure 4). These two rare minerals occur either as late-stage phases during the primary mineralization or as secondary remobilization products.

Galena occurs as large grains and forms together with chalcopyrite, sphalerite, pyrite and secondary tetrahedrite the matrix of the sulfide mineralization. Galena contains many tiny pebble-shaped inclusions. The size of the inclusions is near the limit of the optical resolution. The most important inclusions are freibergite-tetrahedrite$_{ss}$, polybasite and acanthite (Fig. 3).

Chalcopyrite forms large grains, with grain sizes up to a few millimeters but it also occurs as fine inclusions and veins in sphalerite. The small chalcopyrite inclusions in sphalerite are up to 20 microns large, but in many cases only submicroscopic “chalcopyrite dust” was observed. Star-shaped sphalerite inclusions are a widespread texture found in large chalcopyrite grains. The star-shaped sphalerite inclusions are oriented along two, perpendicular, crystallographic directions. Most of the large chalcopyrite grains are characterized by distinct, slightly anisotropic lamellae.

Sphalerite occurs as large grains as well as small star-shaped inclusions in chalcopyrite (Figure 5). The large grains are in many cases dissolved and pervaded by chalcopyrite (Figure 5). The original grain shape of sphalerite is in some cases still visible. A common texture of the large sphalerite grains is the occurrence of numerous pebble-shaped chalcopyrite inclusions. Their sizes range from few tenths of microns down to submicroscopic chalcopyrite “dust”. It was observed that in the inner part of sphalerite cores only a few large chalcopyrite pebbles occur while in the outer rims tiny, almost “dusty”, chalcopyrite inclusions are more common. Adjacent to the pervading chalcopyrite veins sphalerite shows reddish-grey optical zoning.

Pyrite mostly occurs as idiomorphic grains within chalcopyrite. Texturally it is a product of a later, secondary mineralization or remobilization stage since it overgrows other phases and textures. For instance, oriented star-shaped sphalerite inclusions, which occur in chalcopyrite were overgrown by these later-grown pyrites. Reflected light microscopy revealed a weak anisotropy of the pyrite grains.

Secondary tetrahedrite grows interstitially as well as on the crystal faces of idiomorphic pyrite grains. The phase occurs as crack filling and in veins pervading the primary phase assemblage. From this textural appearance seondary tetrahedrite is a product of a secondary mineralization or remobilization stage Secondary tetrahedrite can be distinguished from pebble-shaped primary freibergite-tetrahedriteSS by the textural occurrence and its polygonal grain-shape. The occurrence of freibergite-tetrahedrite$_{ss}$ is restricted to small inclusions in galena.

sample	ga	cp	sph	fah I	fah II	py	plb	ac	el	co/gu
P2a	+	+	+	+	+	+	-	-	-	-
P2b	+	+	+	-	+	+	-	-	-	-
P3	+	+	+	+	+	+	+	+	-	-
P3a	+	+	-	+	+	+	+	-	-	-
P3b	+	+	+	+	+	+	-	-	+	-
P3c	+	+	+	+	+	+	+	-	+	-
P3d	+	+	+	+	+	+	+	+	-	-
P4a	+	+	+	+	-	+	+	+	-	-
P5a	+	+	+	+	+	+	+	-	-	-
P6a	+	+	+	+	+	+	+	+	-	-
P6d	+	+	+	-	+	+	-	-	-	-
P7	-	+	+	-	-	+	-	-	-	-
P7d	+	+	+	+	+	+	+	+	-	-
P9a	-	+	-	-	-	+	-	-	-	-
P9b	-	+	-	-	-	-	-	-	-	+

Table 1: Mineral assemblage of all investigated samples. Abbreviations: ga: galena, cp: chalcopyrite, sph: sphalerite, fah I: freibergite-tetrahedritess, fah II: secondary tetrahedrite, py: pyrite, plb: polybasite, ac: acanthite, el: electrum, co/gu: cosalite gustavite.

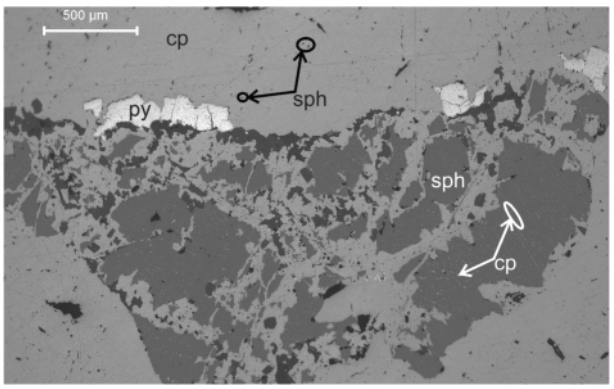

Figure 4: Reflected light microphotograph showing a strongly decomposed sphalerite grain. The primary grain-shape is still visible. Spha-lerite contains numerous chalcopyrite inclusions while the surrounding chalcopyrite grains contain star-shaped sphalerite inclusions. Abbreviations: cp: chalcopyrite, sph: sphalerite.

5. Mineral chemistry

Freibergite-tetrahedrite$_{ss}$: Analyses of freibergite-tetrahedrite$_{ss}$ inclusions in galena were normalized to 13 S+Se per formula unit. Normalized analyses show semimetal excess sums of >4 a.p.f.u. Sb+As when compared to the ideal stoichiometry. The inclusions are rich in Sb and Ag, representing near freibergite end-member compositions. The chemical composition is in contrast to the large fahlore grains intergrown with matrix chalcopyrite, sphalerite, pyrite and galena. The mean As concentration of latter is 0.96 wt.%, equal to 94.5% tetrahedrite end-member. The highest tetrahedrite component is 99.25%. The Ag content of the fahlore inclusions in galena reaches up to 5.67 a.p.f.u. (30.30 wt.% Ag), which is equivalent to a freibergite component of 94.5% (Figure 6). However, Ag concentrations show strong variations down to 0.93 wt.%. The mean Ag concentration is 14.89 wt.%. Another notable chemical feature of the fahlore inclusions are high Cd concentrations. Even if Cd-concentrations <1 wt.% can be attributed to at least in

part to interferences with Ag, the maximal Cd concentrations of 11.20 wt.% indicate uncommonly high Cd concentrations in freibergite-tetrahedrite$_{ss}$. The Cd end-member component ranges from 2.5% to 88% (0.05 a.p.f.u. to 1.76 a.p.f.u.). Some analyses show Au concentrations up to 0.09 wt%, however, considering the detection limit of 300 ppm -400 ppm and the analytical error, this values are not reliable for further interpretation. Chemical analyses of freibergite-tetrahedrite$_{ss}$ are listed in Table 2 (analyses 1-3).

Polybasite: Due to its small grain size electron microprobe analyses was not always possible, however in some cases the grain size of polybasite was large enough for reliable EMPA analyses. The chemical analyses revealed no solid solution between polybasite and the As end-member pearceite, therefore the measured phase represents the Sb end-member. The analyses were normalized to 11 S atoms, according to the general formula of the polybasite-pearceite solid solution $[Ag_9CuS_4][(Ag,Cu)_6(Sb,As)_2S_7]$ by Bindi et al. (2007). The Ag concentration varies between 62.49 wt.% and 74.25 wt.%, this corresponds to 13.87 a.p.f.u. and 20.61 a.p.f.u. (Table 3). The Cu content is low, ranging from 1.93 wt.% to 6.91 wt.%; this corresponds to 0.72 and 2.60 a.p.f.u. (4.52% and 16.27% Cu substitution for Ag). Se substitutes for S with up to 0.75 wt.%. The Sb content ranges from 1.69 to 3.10 a.p.f.u. The As content is near or below the detection limit. As shown in Table 3 Pb concentrations are highly variable and exceed in some EPMA spot analyses 10 wt.%. These values are not to expect as solid solution. In fact these concentrations are mainly analytical artefacts arising from the small grain size of the phase, which occurs basically as inclusion in galena.

Acanthite: Due to the rare occurrence and small grain size of acanthite, only few chemical analyses could be carries out. EDS and WDS analyses revealed pure Ag2S composition.

Electrum: Due to the small grain size only one microprobe analysis of electrum was possible. The Au concentration is 61.67 wt% and the Ag concentration is 35.09 wt%. The composition of electrum is $Au_{49}Ag_{51}$. The analysis also shows traces of Hg (0.95 wt.%).

Cosalite and gustavite are intimately intergrown and form rims surrounding chalcopyrite. The ideal composition of cosalite is $Pb_2Bi_2S_5$. Variable amounts of Cu and Ag can be incorporated (Pring and Etschmann, 2002) according to the following substitution: Pb + [] ↔ Cu + Ag (Pring, 1989). This leads to the general formula $Cu_xAg_xPb_{8-x}Bi_8S_{20}$ (Pring and Etschmann, 2002). Cosalite from the Pfunderer Berg incorporates 2.95 to 2.98 wt.% Ag and 1.35 to 1.48 wt.% Cu. Normalized to 5 S+Se these concentrations correspond to 0.28 a.p.f.u. Ag and 0.21-0.24 a.p.f.u. Cu respectively. Cosalite analyses reveal high Se concentrations, ranging from 0.97 to 1.06 wt.%. The mean cosalite composition fits the formula $Cu_{0.89}Ag_{1.10}Pb_{6.88}Bi_{8.02}S_{19.49}Se_{0.51}$. This composition agrees with the substitution proposed by Pring (1989) where Ag substitutes for Pb and Cu occupies a vacant site. Gustavite shows a more complex stoichiometry, which fits the formula $AgPbBi_3S_6$ and belongs to the lillianite homologous series, a Pb-Bi-(Ag) solid solution of sulfosalts

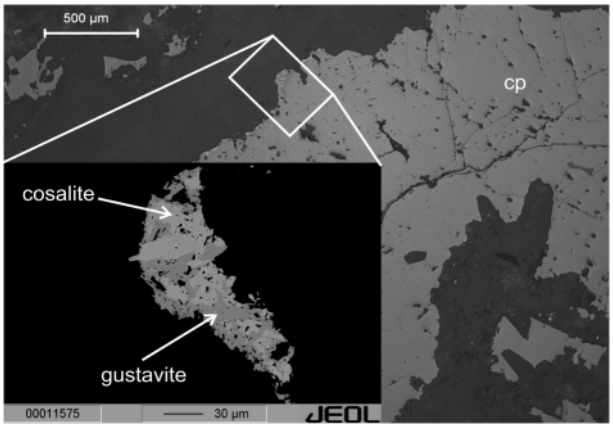

Figure 5: Reflected light microphotograph and backscattered electron image close-up of a gustavite/cosalite rim surrounding chalcopyrite. Abbreviations: co: cosalite, gu: gustavite, cp: chalcopyrite.

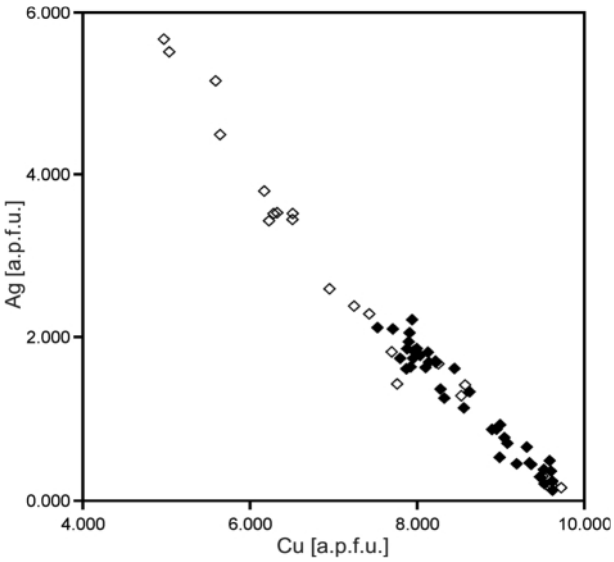

Figure 6: Ag-Cu correlation diagram of electron microprobe analyses of freibergite-tetrahedrite$_{ss}$ inclusions in galena (open diamonds) and secondary tetrahedrite grains, coexisting with pyrite (filled diamonds).

(Pring and Etschmann, 2002). Chemically gustavite can be derived from ideal lillianite $Pb_3Bi_2S_6$ by the substitution Ag + Bi ↔ 2 Pb. Gustavite from the Pfunderer Berg has a composition close to the ideal end-member, but also contains 1.43 wt.% Se, which substitutes for S. The mean chemical composition can be described with the formula $Pb_{1.10}Ag_{0.99}Bi_{2.91}S_{5.78}Se_{0.22}$. Chemical analyses of cosalite and gustavite are given in Table 3.

Galena: Since galena was considered to be the main Ag carrier in the older literature (see Dorfmann 1974), it was one of the aims of this study to verify if galena itself or if the fine inclusions in galena were the Ag carrier. Ag concentrations of galena measured by electron microprobe are in most cases near or below the detection limit. However few single analyses reveal up to 1.15 wt% Ag. The Cd concentration of galena is very low ranging from below the detection limit to 0.26 wt.% with a mean value of 0.06 wt.%. Bi was always detected in galena. The mean concentration of Bi is 0.60 wt.% and the highest concentration reaches 0.81 wt.%.

Chalcopyrite: Large chalcopyrite grains and small chalcopyrite inclusions can be distinguished in terms of their chemical compositions. The maximal Zn concentration in chalcopyrite is 7.43 wt.%. This value was measured in a chalcopyrite inclusion in sphalerite and is probably an analytical artefact due to the small grain size. In contrast, the highest Zn concentration of matrix chalcopyrite is only 1.55 wt.%. This value can considered to be in solid solution within the chalcopyrite lattice. Similar concentrations around 1 wt.% were reported from experiments between 400 and 500°C in the chalcopyrite stability field (Lusk & Calder, 2004) Some important trace elements, detected in chalcopyrite, are Pb, Sn, Zn and Cd. In some cases low In concentrations of up to 0.11 wt.% were measured. EMPA spot analyses of matrix chalcopyrite grains yielded no Sn contents. Only some inclusions in sphalerite show up to 4.5 wt.% Sn. The solubility of stannite in chalcopyrite is high, even if only the α-chalcopyrite solid solution or the Sn-bearing intermediate solid solution (ISS) above ~470°C is capable of elevated Sn concentrations (Moh, 1975). The trace elements Pb and Cd show no preferential behavior for either the inclusions or the large chalcopyrite grains. The Pb content ranges from below the detection limit up to 0.30 wt.% with a mean value of 0.14 wt.% and Cd is even lower, with concentrations ranging from below the detection limit up to 0.22 wt.% with a mean value of only 0.05 wt.%.

sample	P2a	P2a	P2a	P3	P3	P3
spot	fah 1	fah 2	fah 3	fah1	fah2	fah3
As	0.06	0.05	0.01	0.69	0.53	0.44
S	20.44	20.56	21.16	23.94	24.59	24.84
Ag	30.03	29.37	24.66	10.50	2.80	3.12
Cu	15.51	15.80	18.24	30.08	35.20	36.38
Ni	0.00	0.01	0.00	0.00	0.01	0.01
Ge	0.00	0.00	0.01	0.00	0.00	0.01
Pb	0.07	0.23	1.87	0.00	0.06	0.12
Sn	0.15	0.15	0.11	0.00	0.02	0.00
Fe	4.83	4.26	5.29	3.48	3.89	3.17
Zn	1.32	1.80	0.32	3.58	3.54	4.18
Se	0.01	0.00	0.03	0.00	0.02	0.00
Sb	26.61	26.88	26.58	27.91	29.16	28.58
In	0.11	0.13	0.08	0.08	0.11	0.07
Co	0.00	0.00	0.01	0.00	0.00	0.00
Te	0.00	0.00	0.00	0.00	0.00	0.00
Au	0.07	0.00	0.09	0.03	0.00	0.03
Cd	0.44	0.47	0.60	0.16	0.11	0.13
Bi	0.00	0.05	0.01	0.00	0.09	0.03
Hg	0.00	0.00	0.02	0.03	0.00	0.00
Mo	0.01	0.01	0.01	0.13	0.01	0.01
Mn	0.00	0.00	0.03	0.00	0.00	0.00
Total	99.66	99.76	99.12	100.60	100.15	101.13
As	0.015	0.013	0.001	0.160	0.119	0.099
S	12.998	13.000	12.993	13.000	12.995	13.000
Ag	5.666	5.510	4.493	1.692	0.439	0.484
Cu	4.968	5.032	5.641	8.227	9.369	9.590
Ni	0.000	0.003	0.000	0.000	0.004	0.003
Ge	0.000	0.000	0.003	0.000	0.000	0.003
Pb	0.006	0.022	0.177	0.000	0.005	0.010
Sn	0.026	0.025	0.018	0.000	0.003	0.000
Fe	1.760	1.544	1.862	1.083	1.178	0.951
Zn	0.411	0.557	0.096	0.952	0.916	1.071
Se	0.002	0.000	0.007	0.000	0.005	0.000
Sb	4.449	4.468	4.290	3.984	4.051	3.932
In	0.020	0.022	0.014	0.012	0.017	0.010
Co	0.000	0.001	0.002	0.000	0.000	0.000
Te	0.000	0.000	0.000	0.000	0.000	0.000
Au	0.007	0.000	0.009	0.003	0.000	0.002
Cd	0.080	0.084	0.105	0.024	0.016	0.020
Bi	0.000	0.005	0.001	0.000	0.007	0.003
Hg	0.000	0.000	0.002	0.002	0.000	0.000
Mo	0.003	0.001	0.002	0.023	0.002	0.002
Mn	0.001	0.001	0.010	0.000	0.000	0.000
semimetals	4.484	4.509	4.309	4.156	4.194	4.046
Fe+Zn+Cd	2.252	2.185	2.063	2.059	2.110	2.041
Ag+Cu	10.634	10.542	10.134	9.919	9.808	10.074

Table 2: Selected electron microprobe analyses of fahlore. Analyses are normalized to 13 S+Se atoms. Fahlore analyses from sample P2a are Ag-rich fahlore inclusions in galena while analyses from sample P3 are secondary tetrahedrite analyses.

Sphalerite shows a complex chemical composition in the system (Zn,Fe,Cu)S. The composition of sphalerite is characterized by strong variations in its Cu and Fe contents as well as relatively high Cd concentrations. The mean Fe content in sphalerite is 7.07 wt.% and Fe ranges from 0.61 wt.% to 12.79 wt.%. Cu ranges from below the detection limit up to 11.68 wt.% with a mean value of 2.13 wt.%. The highest Fe and Cu concentrations derive from one sphalerite analysis which shows masses of fine chalcopyrite inclusions. The inner parts of the sphalerite grains contain large chalcopyrite pebbles and are nearly Cu-free (<0.01 a.p.f.u.) while the Fe concentrations range between 0.15 a.p.f.u. and 0.18 a.p.f.u. The reddish rims and grain boundaries along chalcopyrite-bearing veins contain 0.07 a.p.f.u. to 0.09 a.p.f.u. Cu and ca. 0.10 a.p.f.u. Fe. The latter show a positive near 1:1 correlation of Fe and Cu suggesting the presence of sub-microscopic chalcopyrite inclusions and/or sub surface (approx. ≤ 10µm below) chalcopyrite pebbles which were activated by the electron beam. The mean Cd concentration is 0.51 wt.% but values up to 0.74 wt.% were measured. Chemical analyses of sphalerite are shown in Table 4, analyses 1-2 are Fe-rich and Cu poor, analyses 3-4 are Fe- and Cu-poor and analyses 5-6 are Fe- and Cu-rich.

Pyrite shows besides the main elements Fe and S only trace element concentrations at or below the detection limit. The observed anisotropic behavior of pyrite is not caused by the incorporation of additional elements (e.g. As).

Secondary tetrahedrite is poorer in Ag and Cd compared to the freibergite-tetrahedritess inclusions. The As concentration is higher compared to the inclusions but still low with a mean value of 2.35 wt.%, corresponding to 0.52 a.p.f.u. (equivalent to 13% tennantite end-member). The Ag content varies between 0.79 wt.% and 13.23 wt.%; this corresponds to 0.12 a.p.f.u. and 2.22 a.p.f.u. (2% and 37% freibergite end-member). Pb, Sn and In were detected only in trace concentrations. The maximal measured Pb concentration is 0.30 wt.%. The Sn concentrations are similar to the Pb content. In is present in all analyses, with concentrations between 0.03 wt.% and 0.14 wt.%. Analyses of secondary tetrahedrite are also shown in Table 2 (analyses 4-6).

6. Micro-Raman spectroscopy

Freibergite-tetrahedrite$_{ss}$ inclusions in galena were also ana-

lyzed using micro-Raman spectroscopy and the data were compared to literature data (Table 5). The characteristic bands of freibergite-tetrahedrite$_{ss}$ inclusions in galena from the Pfunderer Berg are similar to the spectra of pure tetrahedrite (Table 5, samples J22 and M11) from Kharbish et al. (2007). Freibergite-tetrahedrite$_{ss}$ inclusions in galena contain elevated Ag and occasionally Cd concentrations. Despite this chemical difference, the Raman bands are comparable to the Sb-rich, Ag-poor samples from Kharbish et al. (2007). However all modes are shifted to slightly lower wavenumbers (Table 5). According to Johnson et al. (1988), Ag substitutes for Cu on the trigonal planar sites located in the cavity of the tetrahedral framework. This substitution increases the length of the six trigonal planar (Cu, Ag)S_3 groups, the so-called spinner blades (Johnson et al. 1988). Thus the framework extends by rotating the (Fe,Zn,Cu, Cd)S_4 tetrahedrons, which is accompanied by a slight increase of the (Sb,As)-S bond length. The result is a shift in the characteristic stretching and bending vibrations of the “cups” of the (Sb,As)S_3 pyramids.

sample	P9b	P9b	P9b	P9b	P3a	P3a
spot	gustavite 2	gustavite 3	cosalite 1	cosalite 2	polybasite 3	polybasite 4
As	0.00	0.02	0.00	0.00	0.02	0.00
S	15.97	16.05	15.41	15.72	14.33	13.77
Ag	9.30	9.40	2.98	2.95	65.55	64.43
Cu	0.31	0.88	1.48	1.35	5.77	2.15
Ni	0.00	0.01	0.04	0.00	0.00	0.00
Ge	0.00	0.00	0.00	0.04	0.00	0.01
Pb	19.27	19.65	35.37	35.81	3.64	12.40
Sn	0.00	0.00	0.00	0.00	0.00	0.00
Fe	0.10	0.35	0.00	0.06	0.00	0.01
Zn	0.00	0.00	0.01	0.10	0.06	0.04
Se	1.36	1.34	1.06	0.97	0.76	0.56
Sb	0.42	0.38	0.19	0.20	10.07	8.03
In	0.09	0.10	0.13	0.08	0.19	0.16
Co	0.13	0.00	0.02	0.00	0.00	0.01
Te	0.00	0.01	0.00	0.00	0.00	0.00
Au	0.04	0.00	0.15	0.00	0.00	0.12
Cd	0.00	0.18	0.11	0.32	0.69	0.76
Bi	52.01	52.23	41.55	42.12	0.00	0.11
Hg	0.00	0.00	0.00	0.00	0.01	0.00
Mo	0.28	0.15	0.43	0.48	0.09	0.05
Mn	0.00	0.00	0.00	0.00	0.00	0.00
Total	99.28	100.75	98.92	100.21	101.17	102.61
As	0.000	0.003	0.000	0.000	0.007	0.000
S	5.800	5.804	19.457	19.512	10.770	10.821
Ag	1.002	1.009	1.116	1.086	14.618	15.023
Cu	0.057	0.161	0.941	0.844	2.184	0.851
Ni	0.000	0.003	0.029	0.000	0.000	0.000
Ge	0.000	0.000	0.000	0.024	0.000	0.003
Pb	1.081	1.098	6.899	6.866	0.423	1.505
Sn	0.000	0.000	0.000	0.000	0.000	0.000
Fe	0.020	0.073	0.000	0.046	0.000	0.006
Zn	0.000	0.000	0.003	0.063	0.021	0.016
Se	0.200	0.196	0.543	0.488	0.230	0.179
Sb	0.040	0.036	0.062	0.064	1.990	1.659
In	0.009	0.010	0.046	0.027	0.039	0.035
Co	0.026	0.000	0.010	0.000	0.000	0.002
Te	0.000	0.001	0.000	0.000	0.000	0.000
Au	0.002	0.000	0.030	0.000	0.000	0.016
Cd	0.000	0.019	0.040	0.115	0.148	0.169
Bi	2.893	2.892	8.035	8.007	0.000	0.013
Hg	0.000	0.000	0.000	0.000	0.001	0.000
Mo	0.034	0.018	0.181	0.200	0.023	0.013
Mn	0.000	0.000	0.000	0.000	0.000	0.000

Table 3: Selected electron microprobe analyses of gustavite, cosalite and polybasite. Gustavite and cosalite were only found in sample P9d. Gustavite analyses are normalized to 6 S+Se atoms while cosalite analyses are normalized to 20 S+Se atoms. Polybasite was normalized to 11 S atoms. Polybasite analyses are from sample P3a and normalized to 11 S+Se.

Pyrite: Anisotropic and isotropic pyrite grains were also analyzed with micro-Raman spectroscopy. Marcasite and arsenopyrite spectra from Mernagh and Trudu (1993) show completely different Raman modes. The acquired spectra are comparable to pyrite described by Mernagh and Trudu (1993). The authors distinguished between optically anisotropic and isotropic pyrite, where slightly lower wavenumbers occur in the anisotropic specimen. Raman modes from anisotropic pyrite measured in this investigation are very similar to anisotropic pyrite described by Mernagh and Trudu (1993). The anisotropic effects, clearly nor produced by chemical variations, are probably due to polishing effects as proposed by Libowitzky (1994).

7. Discussion

7.1 Cd-distribution thermometry between galena and sphalerite

Bethke and Barton (1971) reported experimental measurements of the distribution coefficients of Cd, Mn and Se between galena and sphalerite and the distribution of Se between galena and chalcopyrite. They showed that Cd is strongly fractionated into sphalerite and the two solid solutions exhibit Henry law’s behaviour throughout the concentration range found in nature (Bethke and Barton, 1971). The expected concentrations in natural assemblages are therefore only functions of pressure and temperature. Bethke and Barton (1971) found that the pressure effect on this system is insignificant. The investigated temperature range of Bethke and Barton (1971) was 600°C to 800°C. In our samples galena-sphalerite pairs were selected using optical microscopy. Most large sphalerite grains contain numerous chalcopyrite inclusions and thus show complex textural zoning patterns, which makes the application of the Cd-distribution thermometer complicated. In some samples, up to a few hundred microns large, inclusion-free and chemically unzoned sphalerite grains occur enclosed in large galena grains. Statistical examinations of the microprobe

sample	P7d	P7d	P7d	P7d	P7d	P7d
spot	sph 1	sph 2	sph 3	sph 4	sph 5	sph 6
As	0.00	0.00	0.00	0.00	0.00	0.00
S	32.95	32.98	32.03	32.08	32.88	32.72
Ag	0.00	0.00	0.02	0.03	0.02	0.08
Cu	0.12	0.14	0.27	0.30	5.35	4.27
Ni	0.01	0.00	0.00	0.02	0.00	0.00
Ge	0.00	0.00	0.00	0.00	0.00	0.00
Pb	0.17	0.12	0.07	0.15	0.19	0.14
Sn	0.00	0.00	0.00	0.00	0.00	0.03
Fe	8.13	9.49	0.61	0.70	7.01	8.89
Zn	59.00	57.28	66.51	66.96	55.46	55.04
Se	0.01	0.00	0.00	0.00	0.00	0.00
Sb	0.02	0.00	0.00	0.01	0.00	0.00
In	0.07	0.11	0.08	0.06	0.08	0.08
Co	0.04	0.00	0.00	0.00	0.01	0.04
Te	0.00	0.00	0.00	0.00	0.00	0.00
Au	0.00	0.07	0.00	0.00	0.00	0.00
Cd	0.65	0.52	0.73	0.47	0.63	0.54
Bi	0.02	0.00	0.00	0.01	0.04	0.00
Hg	0.00	0.00	0.00	0.00	0.00	0.00
Mo	0.02	0.03	0.15	0.07	0.13	0.05
Mn	0.20	0.24	0.00	0.00	0.01	0.16
Total	101.39	100.97	100.47	100.84	101.81	102.05
As	0.000	0.000	0.000	0.000	0.000	0.000
S	1.000	1.000	1.000	1.000	1.000	1.000
Ag	0.000	0.000	0.000	0.000	0.000	0.001
Cu	0.002	0.002	0.004	0.005	0.082	0.066
Ni	0.000	0.000	0.000	0.000	0.000	0.000
Ge	0.000	0.000	0.000	0.000	0.000	0.000
Pb	0.001	0.001	0.000	0.001	0.001	0.001
Sn	0.000	0.000	0.000	0.000	0.000	0.000
Fe	0.141	0.165	0.011	0.012	0.122	0.156
Zn	0.876	0.850	1.016	1.022	0.826	0.823
Se	0.000	0.000	0.000	0.000	0.000	0.000
Sb	0.000	0.000	0.000	0.000	0.000	0.000
In	0.001	0.001	0.001	0.000	0.001	0.001
Co	0.001	0.000	0.000	0.000	0.000	0.001
Te	0.000	0.000	0.000	0.000	0.000	0.000
Au	0.000	0.000	0.000	0.000	0.000	0.000
Cd	0.006	0.004	0.007	0.004	0.005	0.005
Bi	0.000	0.000	0.000	0.000	0.000	0.000
Hg	0.000	0.000	0.000	0.000	0.000	0.000
Mo	0.000	0.000	0.002	0.001	0.001	0.000
Mn	0.003	0.004	0.000	0.000	0.000	0.003
Cu+Fe	0.143	0.167	0.015	0.017	0.204	0.221

Table 4: Selected electron microprobe analyses of sphalerite. Analyses are normalized to 1 S atom. Analysis one and two are Fe-rich and Cu-poor, analysis three and four are Fe- and Cu-poor and analysis five and six are Fe- and Cu-rich from sample P7d.

technique revealed detection limits near 370 ppm for Cd. Using this microprobe routine, sphalerite analyses yielded Cd concentrations between 0.18 wt.% and 0.73 wt.%, which is well above the detection limit thus yielding only small errors. On the other hand, the Cd concentration measured in galena is much lower, slightly above, near or below the detection limit, and thus large errors between 30% and 70% have to be taken into account based on count rate statistics. The estimated mean temperature of this semiquantitative thermometer is 695°C according to Bethke and Barton (1971) with errors of ±15-20°C. If we include the analytical uncertainties associated with the Cd concentration in galena the error increases up to ±200°C! This results in temperatures between 500°C and 900°C for all calculated pairs.

7.2 T-logfS_2-relations

Some samples are galena-free and can be described in the chemical systems Cu-Fe-S and Cu-Fe-Zn-S. The phase relations in these systems were experimentally examined by Lusk and Bray (2002) and Lusk and Calder (2004). The T-logfS_2 plot in Figure 7 shows the stability field of the Cu-Fe sulfides combined with isopleths showing the FeS content of sphalerite. The isopleths were calculated according to Lusk and Bray (2004) with 2 mol.% CuS and 1, 5, 10, 15, 20 and 25 mol.% FeS in sphalerite (Figure 7). Assuming temperatures >500°C the ISS phase is stable at sulfur fugacities between -1 and -5 logfS_2. Pyrite was a secondary product and thus can be omitted from the primary ore assemblage. In this case it can be assumed that, due to the absence of pyrrhotite, the limiting reaction:

Pyrrhotite + S_2 → Pyrite

does not mark the lower boundary of fS_2

7.3 Cooling textures as evidence for high-T hydrothermal processes

α-β lamellae: Matrix chalcopyrite shows distinct α-β transformation lamellae. These α-β transformation lamellae in chalcopyrite indicate the formation of chalcopyrite at high temperatures and subsequent cooling (Ramdohr, 1975). The α-β transformation temperature of chalcopyrite is ~550°C (Moh, 1975) and decreases gradually with increasing ZnS concentration in chalcopyrite to ~500°C (4 wt.% ZnS) (Moh, 1975). Large chalcopyrite grains from the Pfunderer Berg show Zn contents of ~1.5 wt.% indicating that minimum temperatures of at least 520 – 530°C can be assumed. However unmixing of star-shaped ZnS grains in chalcopyrite modified the ZnS concentration of chalcopyrite.

Star-shaped sphalerite exsolutions: Another cooling phenomenon is the occurrence of star-shaped sphalerite exsolutions in chalcopyrite. Star-shaped sphalerite exsolutions are clearly restricted to high T-deposits (Ramdohr, 1975). They are caused by the higher solubility of ZnS in the α-chalcopyrite modification at temperatures above 500°C±10°C (Moh, 1975; Ramdohr, 1975). The maximal solubility of ZnS in α-chalcopyrite is reached at 850°C and is 15 wt.% ZnS (Moh, 1975). The maximal measured Zn concentration in chalcopyrite from the Pfunderer Berg is 7.43 wt.% which corresponds to 11.07 wt.% ZnS in chalcopyrite. Measured Zn concentrations in matrix chalcopyrite and chalcopyrite inclusions in sphalerite are within the solubility limits of the chalcopyrite-sphalerite phase diagram (Moh, 1975). The described exsolutions yield a minimum temperature of formation of 500°C.

8. Conclusions

8.1 Petrology of the sulfide mineral assemblage

Textural and mineral chemical data strongly suggest a high-T formation of the primary Cu-Fe-Zn-Pb-(Ag) mineral assemblage of the Pfunderer Berg. Large chalcopyrite grains show

numerous star-like sphalerite inclusions and this texture can be interpreted as exsolution during cooling from a ZnS bearing, high-T ISS phase which is consistent with relatively high sulfur fugacities between -1 and -4 log units. This is in agreement with the observation of α-β transformation lamellae in chalcopyrite, indicating the transformation from a structurally different ISS phases to a low-T chalcopyrite phase during cooling. Sphalerite stars were overgrown by idiomorphic, secondary pyrite suggesting that pyrite belongs clearly to a younger crystallization stage. But it is not clear if pyrite was formed during a late stage of the main ore-forming event during the late Permian or an individual, subsequent event such as the Eo-Alpine or Alpine remobilization. Application of the semi-quantitative Cd-distribution thermometer yielded temperatures >500°C consistent with textural observations such as sphalerite exsolutions in chalcopyrite and the α-β transformation lamellae in chalcopyrite which is a product of cooling from above 500°C. Geobarometric investigations, using the sphalerite-pyrrhotite-pyrite geobarometer, could not be applied to the samples due to the absence of pyrrhotite.

As concluded by Exel (1998) and Fuchs (1988) the ore mineralizations are high-T hydrothermal products related to the intrusions of diorites into the basement. Although a precise information about the thermic conditions of formation of the Pfunderer Berg mineralizations have not been published so far. Fuchs (1988) noted that ore petrographical investigations of small mineralizations related to the Permian Brixen Granite yielded at least epi- to meso-thermal conditions (<300°C; Misra, 2000). Our obtained mineral assemblage and textural relations as well as thermometry are in agreement with the previous data but yield hypothermal conditions of at least 500°C for the Pfunderer Berg mineralizations.

Au (electrum) is a common constituent in many epithermal polymetallic vein deposits associated with subvolcanic high-T porphyry Cu-ores (Hedenquist et al., 1998; Bendezú and Fontboté, 2009; Kouzmanov et al., 2009). The geological setting and the mineralization style suggest a similar, smaller scaled genetic model.

8.2 Identification of the Ag carrier

Microprobe analyses of inclusion-free galena show only occasionally measurable Ag concentrations (sporadically up to 1 wt.% in EMPA spot analyses) and BSE images demonstrated the presence of Ag-rich minerals that occur as small inclusions in galena. The most important inclusion in galena is freibergite-tetrahedritess, which is very rich in Ag and Sb, thus representing near freibergite end-member composition. The highest Ag concentration in fahlore is 5.67 a.p.f.u. Other important inclusions are polybasite and acanthite. Since galena has been mentioned in the older literature as the main “Ag carrier” it could be shown in this study that the presence of abundant Ag-rich mineral inclusions alone is responsible for the high Ag concentrations of bulk galena analysis.

		$\nu_{1(tnt)}$	$\nu_{1(tet)}$	ν_2	ν_3	ν_4
P3 fahlore	incl. in galena	-	358	350	320	292
[1]J22	tetrahedrite	-	362	350	324	298
[1]M11	tetrahedrite	-	363	352	327	297
[1]E22	tennantite	381	368	358	337	302
[1]E23	tennantite	380	366	356	336	304
[1]Kharbish et al. (2007)						

Table 5: Comparison bewteen measured Raman modes of fahlore inclusions in galena from the Pfunderer Berg and fahlore Raman modes from Kharbish et al. (2007).

8.3 Implications for ore provenance in prehistoric mining

The comparison between the ore mineral assemblage of pre-

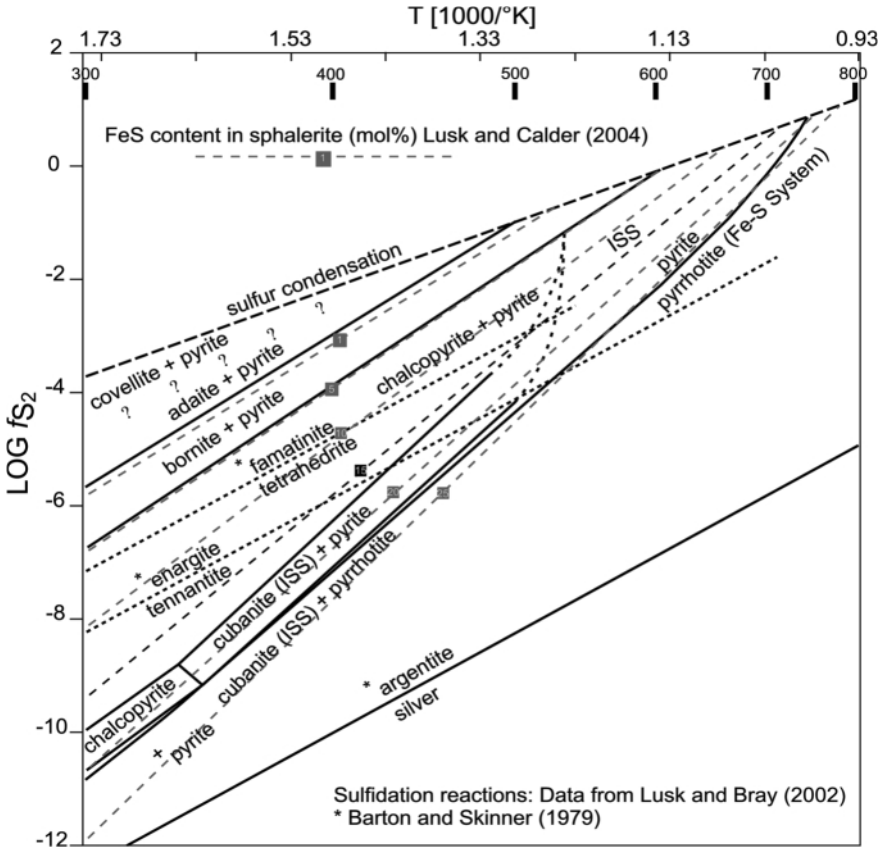

Figure 7: Stability fields of Cu-Fe sulfides in T-logfS_2 space calculated according to Lusk and Bray (2002). The sphalerite isopleths were calculated according to Lusk and Calder (2004) with a CuS concentration of 2 mol.% in sphalerite. The 15 mol.% FeS isopleth is characteristic for an inclusion-free sphalerite from the Pfunderer Berg.

historically mined ore deposits in the Eastern- and Southern Alps clearly shows that chalcopyrite and fahlore-group minerals were the most important phases used in the prehistoric Cu production. The beginning of Cu-metallurgy in the Eastern- and Southern Alps can be dated into the Late Neolithic to Early Bronze Age. Well-known smelting sites are known from the lower Inn valley (North Tyrol, Austria) (Krismer et al., 2009; Bartelheim et al., 2002) and Aqua Fredda from the Trentino (Italy, Metten, 2003). ^{14}C ages from these sites yielded ages of ≥2000 BC. In the Middle- and Late Bronze Age abundant Cu metallurgy in the central Eastern and Southern Alps is known from the Mitterberg (Salzburg, Austria, Stöllner et al., 2006) from Kelchalm/Jochberg/Kitzbühel (North Tyrol, Austria, Goldenberg, 2004), from the Schwaz-Brixlegg mining district (North Tyrol, Austria, Goldenberg and Rieser, 2004) and from the Southern Alps in Trentino (Italy, Metten, 2003). The Pfunderer Berg is geographically located at the intersection between South Alpine and North Alpine smelting and mining sites.

Extensive trace element and Pb-isotope studies from artefacts and ore samples from mining areas from the Northern Greywacke Zone (Mitterberg, Kelchalm/Jochberg/Kitzbühel) were performed by Lutz et al. (2010). They concluded that the deposits of this major Austroalpine unit and especially the Mitterberg were the most important mining districts in the middle- and late Bronze Age. Artioli et al. (2008) presented a similar trace element, Cu-isotope and Pb-isotope database for Cu-mining areas from the Southern Alps (Italian provinces of: Belluno, Trento, South Tyrol). In this study the Pfunderer Berg was considered to be an important Cu-mining area.

In the Mitterberg and the Kelchalm/Jochberg/Kitzbühel mining districts chalcopyrite is the predominant Cu carrier. From the Southern Alps, Metten (2003) reported chalcopyrite to be the most dominant Cu carrier in the smelting site of Aqua Fredda near Trento. So far, the presence of notable amounts of Ag-bearing minerals, associated with chalcopyrite mineralizations has been neglected. The smelting sites from the North Tyrolean Inn Valley on the other hand suggest the processing of fahlore-group minerals with dominantly tetrahedrite-tennantite composition, which resulted in elevated Zn concentrations, the presence of Ag (e.g. fahlore and/or balkanite in Röhrerbühel) and in some cases traces of Co and Ni (tetrahedrite-tennantite with Co and Ni) in the smelting products (Krismer et al., 2009).

The sphalerite- and galena-rich veins of the Pfunderer Berg were probably only of minor interest in prehistoric times but the chalcopyrite-rich domains could have been of considerable interest, although concise archaeological evidence has not been documented yet. The occurrence of evidence for Late Neolithic smelting of sphalerite-galena-chalcopyrite ores from Milland/Brixen, 15 km to the north of the Pfunderer Berg could imply a possible connection to the Pfunderer Berg mineralizations but further investigations are currently being conducted (Artioli et al., 2008; Colpani et al., 2008). Since the chalcopyrite-rich domains contain sphalerite, galena, pyrite and Ag-bearing phases, this would produce slags and raw metals with elevated amounts of Zn, Fe, Pb and Ag phases as well as elemental contents during smelting. The presence of Bi-phases and elevated Bi concentrations in metallurgical products (especially in metal and sulfide phases) can also be expected. Thus during smelting Fe and Zn would form silicates such as Zn-bearing fayalite, Zn-bearing clinopyroxene and Zn-bearing åkermanite/gehlenite (Fe-Si-O slag with Zn) and Ag and Pb would remain similar to As and Sb predominantly in the obtained metal or within distinct sulfide enclaves of the slags and the raw metal (Krismer et al., 2009). Based on elevated Pb (galena), Zn (sphalerite) and Ag (freibergite) contents and minor Bi (cosalite, gustavite) concentrations, the chemical major-, minor- and trace element contents of metallurgical products will show a unique geochemical signature and thus can be probably distinguished from the products of ores from the Trentino and from the North Tyrolean and Salzburg sites.

Acknowledgements

The Financial support through the FWF special research program HiMAT (F3110-G02 to P. T.) is gratefully acknowledged. We thank Anton Beran and Michael Götzinger for their careful review. The manuscript benefitted from the thorough reviews of the journal reviewers A. Beran and M. Götzinger. The editorial handling by Hugh Rice is also gratefully acknowledged.

References

Artioli, G., Baumgarten, B., Marelli, M., Giussani, B., Recchia, S., Nimis, P., Giunti, I., Angelini, I., Omenetto, P., 2008. Chemical and isotopic tracers in alpine copper deposits: geochemical links between mines and metal. Geo Alp, 5, 139-148.

Bartelheim, M., Eckstein, K., Huijsmans, M., Krauss, R. and Pernicka, E. 2002. Kupferzeitliche Metallgewinnung in Brixlegg, Österreich, In: M. Bartelheim, E. Pernicka and R. Krause (eds.), Die Anfänge der Metallurgie in der Alten Welt (The beginnings of metallurgy in the Old World). VML Verlag Marie Leidorf, pp. 33–82.

Barton, Jr., P. B. and Skinner, B. J. 1979. Sulfide mineral stabilities, In: H. L. Barnes, (eds.), Geochemistry of hydrothermal ore deposits, 2nd edition, pp. 278-403.

Bendezú, R., Fontboté, L., 2009. Cordilleran Epithermal Cu-Zn-Pb-(Au-Ag) Mineralization in the Colquijirca District, Central Peru: Deposit-Scale Mineralogical Patterns. Economic Geology, 104, 905-944.

Bethke, P.M., Barton P.B. Jr., 1971. Distribution of some minor elements between coexisting sulphide minerals. Economic Geology, 66, 140-163.

Bindi, L., Evain, M., Spry, P.G., Manchetti, S., 2007. The pearcite-polybasite group of minerals: Crystal chemistry and new nomenclature rules. American Mineralogist, 92, 918-925.

Brigo, L., 1971. Mineralizzazioni e metallogenesi nell' area della Fillade quarzifera di Bressanone nelle Alpi sarentine. Studi Trentini di Sci. Nat. Sez. A, 48, 80-125.

Colpani, F., Angelini, I., Artioli, G., Tecchiati, U. 2008. Copper smelting activities at the Milland and Gudon Chalcolitic sites (Bolzano, Italy): Chemical and mineralogical investigations of the archaeometallurgical finds. Proc. 36th International Symposium on Archaeometry, Quebec, 2-6 May 2006.

Dorfmann, W., 1974. Der Bergbau im Raume Klausen. Dissertation, PhD Thesis, University of Padua, Padua, 146 pp.

Exel, R., 1998. Lagerstättenkundliche und montanhistorische Erhebungen über den Erzbergbau in Südtirol (Provinz Bozen, Italien). Berichte der Geologischen Bundesanstalt (Austria), 42,130.

Fuchs, H. W., 1988. Die transversalen Erzgänge im Gefolge der herzynischen Granitintrusionen in Südtirol. Archiv für Lagerstättenforschung der Geologischen Bundesanstalt (Austria), 9, 19-32.

Goldenberg, G., 2004. Ein Verhüttungsplatz der mittleren Bronzezeit bei Jochberg (Nordtirol), In: Alpenkupfer (Rame delle Alpi) . Der Anschnitt, 17, 165-176.

Goldenberg, G., Rieser, B., 2004. Die Fahlerzlagerstätten von Schwaz/Brixlegg (Nordtirol), In: Alpenkupfer (Rame delle Alpi) . Der Anschnitt, 17, 37-52.

Hoinkes, G., Koller, F., Rantitsch, G., Dachs, E., Hock, V., Neubauer, F., Schuster, R. 1999. Alpine metamorphism of the Eastern Alps. Schweizer Mineralogische Petrographische Mitteilungen, 79, 55-181.

Hendenquist, J. W., Arribas, A. Jr., Reynolds, T. J., 1998. Evolution of an Intrusion-Centered Hydrothermal System : Far Southeast-Lepanto Porphyry and Epithermal Cu-Au Deposits, Philippines. Economic Geology, 93/4, 373-404.

Johnson, N.E., Craig, J.R., Rimstidt, J.D., 1988. Crystal chemistry of tetrahedrite. American Mineralogist, 73, 389-397.

Kharbish, S., Libowitzky, E., Beran, A., 2007. The effect of As-Sb substitution in the Raman spectra of tetrahedrite-tennantite and pyrargyrite-proustite solid solutions. European Journal Mineralogy, 19, 567-574.

Klebelsberg, R., 1935. Geologie von Tirol. Bornträger, Berlin, 872 pp.

Krismer, M., Vavtar, F., Tropper, P., 2008. Thermometry of the intrusion-associated late Permian Pb-Cu-Zn deposit from the Pfunderer berg near Klausen (South Tyrol, Italy). Deutsche Mineralogische Gesellschaft (conference abstract), pp. 185.

Krismer, M., Töchterle, U., Goldenberg, G., Vavtar, F., Tropper, P., Lutz, J., Pernicka, E., 2009. A mineralogical and petrological view at early Bronze Age copper slags from the Kiechlberg (North Tyrol, Austria). In: B. Holzner and M.D. Tilmann (eds.), Mining in European History (conference abstract), Innsbruck University Press, pp.39-40.

Kouzmanov, K., Moritz, R., von Quadt, A., Chiaradia, M., Peytcheva, I., Fontignie, D., Ramboz, C., Bogdanov, K., 2009. Late Cretaceouse porphyry Cu and epithermal Cu-Au association in the Southern Panagyurishte District, Bulgaria: the paired Vlaykov Vruh and Elshitsa deposits. MIneralium Deposita, 44, 611-646.

Libowitzky, E., 1994. Anisotropic pyrite: A polishing effect. Physics and Chemistry of Minerals, 21, 97-103.

Lusk, J., Bray, D.M., 2002. Phase relations and the electrochemical determination of sulphur fugacity for selected reactions in the Cu-Fe-S and Fe-S systems at 1 bar and temperatures between 185°C and 460°C. Chemical Geology, 192, 227-248.

Lusk, J., Calder B.O.E., 2004. The composition of sphalerite and associated sulfides in reactions of the Cu-Fe-Zn-S, Fe-Zn-S and Cu-Fe-S systems at 1 bar and temperatures between 250 and 535°C. Chemical Geology, 203, 319-345.

Lutz, J., Pernicka, E., Pils, R., Tomedi, G., Vavtar, F., 2010. Geochemical characteristics of copper ores from the Greywacke Zone in the Austrian Alps and their relevance as a source of copper in prehistoric times. In press.

Mernagh, T.P., Trudu, A.G., 1993. A laser Raman microprobe study of some geologically important sulphide minerals. Chemical Geology, 103, 113-127.

Metten, B., 2003. Beitrag zur spätbronzezeitlichen Kupfermetallurgie im Trentino (Südalpen) im Vergleich mit anderen prähistorischen Kupferschlacken aus dem Alpenraum. Metalla, 10, 1-122.

Misra, K., C., 2000. Understanding ore deposits. Kluwer Academic Publishers, Dordrecht, 845 pp.

Moh, G.H., 1975. Phase relations and mineral assemblages in the Cu-Fe-Zn-Sn-S system. Chemie der Erde, 34,1-61.

Moll K. E. v. Frh., 1798. Nachrichten von dem Kaiserl.Königl. und zum Teil Gewerkschäftl. Bley-Silber- und Kupferberg- und Schmelzwerk zu Klausen in Tyrol. Moll´s Jahrbücher der Berg- und Hüttenkunde, pp. 116-155.

Niederschlag, E., Pernicka, E., Seifert, Th., Bartelheim, M., 2003. The Determination of Lead Isotope Ratios by Multiple Collector Icp-Ms: A Case Study of Early Bronze Age Artefacts and their Possible Relation With Ore Deposits of the Erzgebirge. Archaeometry, 45, 61-100.

Oeggl, K., Mathis, F., Moser, J., Schneider, I., Leitner, W., Tomedi, G., Stöllner, T., Krause, R., Pernicka, E., Tropper, P., Schibler, J., Nicolussi, K., Hanke, K., 2008. The history of mining activities in the Tyrol and adjacent areas: impact on environment and human societies (HiMAT). Antiquity, 82, 317.

Posepny, F., 1880. Die Erzlagerstätten am Pfunderer Berg bei Klausen in Tirol. Archiv für praktische Geologie, Band 1, pp. 441-487.

Pring, A., 1989. Structural disorder in aikinite and krupkaite. American Mineralogist, 74, 250-255.

Pring, A., Etschmann, B., 2002. HRTEM observations of structural and chemical modulations in cosalite and its relationship to the lillianite homologues. Mineralogical Magazine, 66, 451-458.

Ramdohr, P., 1975. Die Erzmineralien und ihre Verwachsungen, Akademie Verlag, Berlin, 1277 pp.

Sassi, F.P., Spiess, R., 1993. The Southalpine metamorphic basement in the Eastern Alps. In: J.F. Raumer and F. Neubauer, (eds.), The pre-Mesozoic Geology in the Alps. Springer, Berlin, pp. 599-607.

Stöllner, T., Cierny, J., Eibner, C., Boenke, N., Herd, R., Maass, A., Röttger, K., Sormaz, T., Steffens, G., Thomas, P., 2006. Der Bronzezeitliche Bergbau im Südrevier des Mitterberggebietes. Bericht zu den Forschungen der Jahre 2002 bis 2006. Archaeologia Austriaca, 90, 87-137.

Received: 19 April 2010
Accepted: 20 January 2011

Matthias KRISMER*), Franz VAVTAR, Peter TROPPER, Bernhard SARTORY & Reinhard KAINDL

Institute of Mineralogy and Petrography, Faculty of Geo- and Atmospheric Sciences, University of Innsbruck, Innrain 52, A-6020 Innsbruck, Austria;

*) Corresponding author, matthias.krismer@uibk.ac.at